PHYSICAL REVIEW D **87,** 114514 (2013)

Finite temperature study of the axial U(1) symmetry on the lattice with overlap fermion formulation

Guido Cossu,[1] Sinya Aoki,[2,3] Hidenori Fukaya,[4] Shoji Hashimoto,[1,5] Takashi Kaneko,[1,5] Hideo Matsufuru,[1] and Jun-Ichi Noaki[1]

[1]*Theory Center, IPNS, High Energy Accelerator Research Organization (KEK), Tsukuba 305-0810, Japan*
[2]*Yukawa Institute for Theoretical Physics, Kyoto University, Kitashirakawa Oiwakecho, Sakyo-ku, Kyoto 606-8502, Japan*
[3]*Center for Computational Sciences, University of Tsukuba, Tsukuba, Ibaraki 305-8577, Japan*
[4]*Department of Physics, Osaka University, Toyonaka 560-0043, Japan*
[5]*School of High Energy Accelerator Science, The Graduate University for Advanced Studies (Sokendai), Tsukuba 305-0801, Japan*

(Received 30 April 2013; published 27 June 2013; corrected 8 July 2013)

We examine the axial U(1) symmetry near and above the finite-temperature phase transition in two-flavor QCD using lattice QCD simulations. Although the axial U(1) symmetry is always violated by quantization, i.e., the chiral anomaly, the correlation functions may manifest effective restoration of the symmetry in the high-temperature phase. We explicitly study this possibility by calculating the meson correlators as well as the Dirac operator spectral density near the critical point. Our numerical simulations are performed on a $16^3 \times 8$ lattice with two flavors of dynamical quarks represented by the overlap fermion formalism. Chiral symmetry and its violation due to the axial anomaly is manifestly realized with this formulation, which is a prerequisite for the study of the effective restoration of the axial U(1) symmetry. In order to avoid discontinuity in the gauge configuration space, which occurs for the exactly chiral lattice fermions, the simulation is confined in a fixed topological sector. It induces a finite-volume effect, which is well described by a formula based on the Fourier transform from the θ vacua. We confirm this formula at finite temperature by calculating the topological susceptibility in the quenched theory. Our two-flavor simulations show degeneracy of the meson correlators and a gap in the Dirac operator spectral density, which implies that the axial U(1) symmetry is effectively restored in the chirally symmetric phase.

DOI: 10.1103/PhysRevD.87.114514 PACS numbers: 12.38.Gc, 11.30.Rd, 12.38.Aw

I. INTRODUCTION

Chiral symmetry plays a key role in understanding the nature of the vacuum of quantum chromodynamics (QCD). With N_f flavors of massless quarks, the QCD Lagrangian has a symmetry $\mathrm{U}(N_f)_L \otimes \mathrm{U}(N_f)_R$ under field rotations involving flavor mixings for left-handed and right-handed quarks independently. Among them the flavor-singlet part of the chiral (or axial) transformation, which forms $\mathrm{U}(1)_A$, is violated by quantization. This is known as the chiral or axial anomaly. At zero temperature, the remaining symmetry $\mathrm{SU}(N_f)_L \otimes \mathrm{SU}(N_f)_R \otimes \mathrm{U}(1)_V$ is spontaneously broken down to $\mathrm{SU}(N_f)_V \otimes \mathrm{U}(1)_V$, and $N_f^2 - 1$ massless Nambu-Goldstone bosons appear. At finite temperature, in the massless limit, a restoration of symmetry is expected back to $\mathrm{SU}(N_f)_L \otimes \mathrm{SU}(N_f)_R \otimes \mathrm{U}(1)_V$ above a critical temperature T_c.

This symmetry breaking and its restoration are characterized by a vacuum expectation value of a flavor-singlet scalar operator $\bar{q}q$, which is called the chiral condensate $-\langle\bar{q}q\rangle \equiv \Sigma$, the order parameter of this phase transition. According to the Banks-Casher relation [1]

$$\Sigma = \pi\rho(0), \tag{1}$$

a nonzero chiral condensate implies an accumulation of low-lying eigenvalues of the Dirac operator D. Here, $\rho(\lambda)$ is a spectral density of D defined as $\rho(\lambda) = (1/V)\sum_{\lambda'}\langle\delta(\lambda - \lambda')\rangle$ with V a four-volume of space-time and $\langle\cdots\rangle$ denotes an expectation value. The Banks-Casher relation (1) is satisfied in the thermodynamical limit, i.e., infinite-volume limit, followed by the limit of vanishing quark mass. This implies that the density of low-lying eigenvalues of D must disappear above the transition temperature.

The chiral anomaly is reflected in the particle spectrum (in the low-temperature phase) as a mass-splitting of the corresponding pseudoscalar meson, the η meson in the case of $N_f = 2$ for example, from the flavor nonsinglet pseudoscalar particles, i.e., π mesons. In terms of (valence) quark-flow diagrams, the difference between flavor-singlet and -nonsinglet mesons comes from a disconnected diagram in the meson two-point correlation functions. It is found that the main contribution to the disconnected diagram is from low-lying quark eigenmodes if one decomposes the quark propagator into the contributions of individual eigenmodes of the Dirac operator [2]. An interesting question then emerges: above the finite-temperature phase transition, where we expect the suppression (or even absence) of the low-lying eigenmodes, does η become degenerate with flavor-nonsinglet pseudoscalars? If so, the axial U(1) symmetry is effectively restored at least in the particle spectrum at high temperature. This

may have a significant impact on the nature of the finite-temperature phase transition, since the symmetry controls the order and critical exponents of the phase transition [3].

Such an argument was originally made by Cohen [4], followed by several theoretical studies [5–9]. A numerical study using lattice QCD, on the other hand, has been missing, because most numerical simulations at finite temperature performed so far used the staggered fermion formulation, which realizes chiral symmetry only partially. An even more important problem of the staggered fermion is in the so-called *rooting* procedure, i.e., a square root of the fermion determinant is taken to represent two flavors of light quarks in nature out of four artificial flavors built in the staggered fermion. The flavor-singlet axial transformation is ill defined in such a theory. With this caveat, there was a recent study of the Dirac spectral density using the staggered fermion [10]. In this paper, we present the first numerical study of this problem employing the overlap fermion formulation [11,12], for which the full flavor and chiral symmetries are realized on the lattice including the flavor-singlet axial symmetry existing at the Lagrangian level and violated by quantization.

Although the numerical cost for the simulation of the overlap fermion is substantially higher than that of the staggered fermion, its simulation has become feasible by recent developments of machines and algorithms, and in fact has been extensively performed by the JLQCD and TWQCD collaborations in the past years [13]. The overlap fermion is constructed with the overlap Dirac operator D_{ov},

$$D_{\mathrm{ov}} = m_0[1 + \gamma_5 \mathrm{sgn}(H_W(-m_0))], \tag{2}$$

where $H_W(-m_0)$ is the Hermitian Wilson-Dirac operator $H_W(-m_0) = \gamma_5 D_W(-m_0)$ with a large negative mass $-m_0$, which is of order of the lattice cutoff. This operator satisfies the Ginsparg-Wilson relation [14], $D_{\mathrm{ov}}\gamma_5 + \gamma_5 D_{\mathrm{ov}} = D_{\mathrm{ov}}\gamma_5 D_{\mathrm{ov}}/m_0$, through which the exact chiral symmetry on the lattice can be defined [15]. The operator (2) has a singularity due to the sign function, when an eigenvalue of $H_W(-m_0)$ crosses zero as the background gauge field varies. This corresponds to a boundary between two adjacent topological sectors of the gauge field. A numerical simulation with currently available algorithms becomes prohibitively costly when one crosses this singularity; the JLQCD and TWQCD collaborations took a strategy to fix the topological sector during the Monte Carlo simulation. Physical quantities at the $\theta = 0$ vacuum are reconstructed later by correcting the finite-volume effect of $O(1/V)$ due to fixing the topology [16,17].

Since the artifact due to fixing topology is essentially a finite-volume effect, the same strategy should work at finite temperature as far as the spatial volume is sufficiently large. Detailed discussions are given in Sec. II. We numerically check this property by calculating the topological susceptibility on quenched lattices, which is given in Sec. III. As discussed in Ref. [17], even when the global topology is fixed, local topological fluctuations are still active and the topological susceptibility can be extracted from a long-range correlation of topological charge densities. The results at finite temperature obtained in this work are compared with conventional calculations from the fluctuation of global topology found in the literature.

We then discuss the results of our exploratory simulations of two-flavor QCD at finite temperature using the overlap fermion formulation in Sec. IV. The global topological charge is fixed to zero. We analyze the low-lying eigenvalue spectral density of the overlap Dirac operator, as well as the meson correlators to investigate the effective restoration of the axial U(1) symmetry. Both connected and disconnected parts of the correlator are reconstructed from the low-lying eigenmodes, which are calculated and stored in advance. The disconnected part produces the difference between the meson channels related by the $\mathrm{U}_A(1)$ symmetry transformations. We show that, in the high-temperature phase, the disconnected contribution is indeed vanishing towards the chiral limit of sea quarks.

A similar study of the restoration of the axial U(1) symmetry has recently been made by the HotQCD collaboration [18] using the domain-wall fermion formalism. Like the overlap fermion, the domain-wall fermion realizes exact chiral symmetry on the lattice, but only in the limit of an infinitely large fifth dimension. In practical simulations, the chiral symmetry is slightly violated and an additive mass renormalization m_{res} appears. The size of m_{res} is typically on the order of MeV, and poses a significant problem when one tries to identify the near-zero eigenvalues, which are of the same order or even lower. The overlap fermion employed in this work enables a clear identification of the near-zero modes and their effects on the physical quantities.

Reports of our work at earlier stages are found in Refs. [19,20].

II. PHYSICS AT FIXED TOPOLOGY

In QCD, the fluctuation of global topology Q is necessary to guarantee the cluster decomposition property, which is one of the fundamental conditions necessary in constructing a meaningful quantum field theory. It is easy to see that the different topological sectors have to be added with a weight of the form $e^{i\theta Q}$, through which the QCD θ parameter is defined [21]. The formulas to relate the physical quantities obtained in a fixed topological sector Q to those in the $\theta = 0$ vacuum were developed in Refs. [16,17]. They are valid also at finite temperature as outlined below.

Let $Z(\theta)$ be a partition function of QCD with the θ term put in a volume $V = L^3 \times \beta$. Here, L and β are the spatial and temporal extent of the box respectively ($\beta = N_t a$). The partition function Z_Q at a fixed global topological charge Q can be written as a Fourier transform of the θ vacua,

$$Z_Q = \frac{1}{2\pi}\int_{-\pi}^{\pi} d\theta Z(\theta)\exp(i\theta Q) = \frac{1}{2\pi}\int_{-\pi}^{\pi} d\theta \exp(-\beta F(\theta)L^3), \quad (3)$$

where $F(\theta) \equiv E_0(\theta) - i\theta Q/V$.

Near zero temperature, $E_0(\theta)$ represents the vacuum energy density, $Z(\theta) = \exp(-\beta E_0(\theta)L^3)$. The integral in Eq. (3) may be evaluated using the saddle-point expansion around

$$\theta_c = i\frac{Q}{\chi_t V}(1 + O(\delta^2)), \quad (4)$$

where χ_t is defined through an expansion of $E_0(\theta)$ in terms of θ,

$$E_0(\theta) = \sum_{k=1}^{\infty}\frac{c_{2k}}{(2k)!}\theta^{2k} = \frac{\chi_t}{2}\theta^2 + O(\theta^4), \quad (5)$$

and $\delta \equiv Q/(\chi_t V)$. The result up to small δ^2 terms is given by

$$Z_Q = \frac{1}{\sqrt{2\pi\chi_t V}}\exp\left(-\frac{Q^2}{2\chi_t V}\right) \times\left[1 - \frac{c_4}{8V\chi_t^2} + O\left(\frac{1}{V^2}, \delta^2\right)\right]. \quad (6)$$

The global topological charge distributes as a Gaussian with a width specified by the topological susceptibility χ_t. At finite volume, the correction appears at order $1/V$. The basic assumption in obtaining Eq. (6) through the saddle-point expansion is that $E_0(\theta)$ takes its minimum value at $\theta = 0$ and is analytic around there.

At nonzero temperature, β plays the role of inverse temperature. As the first excited-state energy $E_1(\theta)$ becomes significant compared to the temperature, $\beta(E_1(\theta) - E_0(\theta))L^3 \sim 1$, the partition function $Z(\theta)$ receives contributions from the excited states as $Z(\theta) = \sum_n \exp(-\beta E_n(\theta)L^3)$, and the relation (3) has to be modified to include them. This can be done by redefining the "energy" as $\beta\tilde{E}(\theta)L^3 \equiv -\ln Z(\theta)$ and accordingly the "free energy" $\beta\tilde{F}(\theta)L^3 \equiv \beta\tilde{E}(\theta)L^3 - i\theta Q/V$. As far as the analyticity property of $\tilde{E}(\theta)$ around $\theta = 0$ is unchanged, the same saddle-point approximation can be applied, and Eq. (6) is valid with χ_t and c_4 evaluated at finite temperature. The condition that $1/V^2$ and δ^2 have to be small in Eq. (6) is still applied. Since β is fixed, the condition implies a large spatial volume L^3 to make $V = \beta L^3$ sufficiently large.

The same conclusion is obtained by considering the "energy" defined through a transfer matrix in one of three spatial directions. In this way, the spatial extent L plays the role of inverse temperature and the whole argument given at vanishing temperature remains unchanged. Again, the volume V appearing in the formulas is the space-time volume βL^3.

Along the same line of argument, one can obtain the relation between correlation functions at fixed Q and those at fixed θ. For instance, for a correlator $G(\theta)$ that is CP even at $\theta = 0$, one obtains [17]

$$G_Q = G(0) + G^{(2)}(0)\frac{1}{2\chi_t V}\left[1 - \frac{Q^2}{\chi_t V} - \frac{c_4}{2\chi_t^2 V}\right] + G^{(4)}(0)\frac{1}{8\chi_t^2 V^2} + O(V^{-3}). \quad (7)$$

Namely, the correlator at a fixed topology G_Q is written in terms of $G(0)$ and its second derivative $G^{(2)}(0) \equiv dG(\theta)/d\theta|_{\theta=0}$, and so on. The first correction is again of the order of $1/V$.

One important example of Eq. (7) is that for a two-point correlation function of the topological charge density $\omega(x)$. It can also be written in terms of flavor-singlet pseudoscalar density operators $mP(x)$ using the flavor-singlet axial-Ward-Takahashi identity. Fixing the global topology, a constant correlation remains at long distances,

$$\lim_{|x|\to\text{large}}\langle mP(x)mP(0)\rangle_Q = \frac{1}{V}\left(\frac{Q^2}{V} - \chi_t - \frac{c_4}{2\chi_t V}\right) + O(e^{-m_\eta|x|}). \quad (8)$$

At finite temperature, the long distance $|x|$ must be taken in the spatial direction.

The constant correlation appearing in Eq. (8) is understood as the effect of fixing the topology. Let us consider a sector of $Q = 0$, as an example, i.e., the global topology is constrained to zero. If there is a positive topological charge fluctuation locally near the origin, there would be more chance to find a negative fluctuation apart from there in order that $\langle mP(x)\rangle$ is summed up to zero when integrated over space-time. The correlation $\langle mP(x)mP(0)\rangle$ is thus negative at long distances and is proportional to the ability to have local topological fluctuations, which is characterized by χ_t. Since the effect must vanish on a large enough volume, one expects a contribution of the form $-\chi_t/V$.

The relation (8) suggests a possibility to extract χ_t from the measurement done in the fixed topology. Indeed, it was successfully performed at zero temperature in Ref. [2].

The last term in Eq. (8) represents a physical correlation due to the flavor-singlet pseudoscalar particle, here denoted as η. In the lattice calculation of the flavor-singlet correlation functions, there appear connected and disconnected quark-flow diagrams. Both diagrams contain a slow decay mode due to the flavor-nonsinglet pion, which cancels between the two diagrams, and only the rapidly decaying channel of heavier η particles remains. In the quenched theory, there is no pion component in the disconnected sector and a modified contribution from the so-called hairpin diagram has to be considered, as discussed later in Sec. III C.

When χ_t is very small, which is expected for $N_f = 2$ QCD above T_c, our method for extracting χ_t is no longer valid. However, the disconnected propagator is still useful since its absence (or presence) itself is a signal for the $U_A(1)$ restoration (or breaking). If there is a sizable gap in the Dirac spectral density, it is likely that the disconnected diagram is highly suppressed and $\chi_t = 0$. Conversely, if the eigenvalue density is nonzero but very tiny, χ_t is likely to have a nonzero value. In this way, even when χ_t is small, we can indirectly investigate whether $\chi_t = 0$ or not, and $U_A(1)$ is restored or not, through the fixed-topology simulations.

III. STUDY OF FIXED TOPOLOGY IN QUENCHED QCD

Before performing two-flavor QCD simulations at finite temperature, we carry out a quenched study in order to validate the strategy of extracting the physics of the $\theta = 0$ vacuum from the fixed topology simulations at finite temperature. We measure the topological susceptibility at finite temperature using the method outlined in the previous section and compare the results with those in the literature obtained with the conventional method of calculating the variance of the global topological charge $\langle Q^2 \rangle$.

A. Setup and data sets

In order to fix the global topological charge throughout the hybrid Monte Carlo (HMC) simulation, the JLQCD collaboration introduced two extra species of unphysical Wilson fermions with a large negative mass $-m_0$ [22]. With the mass of order of the lattice cutoff, the extra degrees of freedom are irrelevant in the continuum limit. Since the overlap Dirac operator $D_{\rm ov}$ is built upon the Hermitian Wilson-Dirac operator $H_W(-m_0)$ as in Eq. (2), a change of the index of $D_{\rm ov}$ accompanies a zero-crossing of one of the eigenvalues of $H_W(-m_0)$. The extra Wilson fermions generate a fermion determinant of the form $\det[H_W(-m_0)^2]$ and such a zero-crossing is prohibited. We also introduce twisted-mass ghosts to cancel unwanted contributions from the extra Wilson fermions. The net effect for the Boltzman weight in the path integral is

$$\frac{\det[H_W(-m_0)^2]}{\det[H_W(-m_0)^2 + \mu^2]}, \tag{9}$$

where μ is the twisted mass given to the ghosts. The eigenmodes of $|H_W(-m_0)|$ above μ do not contribute to the Boltzman weight effectively, and only the near-zero modes are affected. In this work, we chose $\mu = 0.2$ in the lattice unit.

The suppression of the near-zero modes of $H_W(-m_0)$ does not spoil local topological fluctuations that give rise to the topological susceptibility χ_t. Indeed, using the same formulation, χ_t was successfully calculated and confirmed to be consistent with the expectation from chiral perturbation theory [2].

We generated finite-temperature data in the pure gauge theory on a lattice of size $24^3 \times 6$. With $N_t = 6$, the transition temperature corresponds to the lattice spacing $a \simeq 0.11$ fm, which is in the region where the locality of the overlap-Dirac operator is satisfied with our choice of lattice actions. We take a range of lattice spacing 0.09–0.13 fm, which corresponds to $\beta = 2.35$–2.55 with the Iwasaki gauge action. The lattice spacing is estimated from the heavy-quark potential measured on independent zero-temperature lattices with an input of $r_0 = 0.49$ fm. For each parameter, we accumulated $O(300$–$500)$ configurations separated by 50–100 HMC trajectories in the trivial topological sector $Q = 0$. The lattice parameters are summarized in Table I.

The autocorrelation time of standard thermodynamical observables, like internal energy and the order parameters, the Polyakov loop and chiral condensate, are negligible. The decorrelation of topology-related quantities, such as the lowest eigenvalue of the overlap Dirac operator, is very slow at higher temperatures, which is a well known effect on fine lattices (see for example Refs. [24,25]).

We estimate the finite-temperature phase transition point T_c by an inflection point of the Polyakov loop, which is more precise than its susceptibility with our statistics. The corresponding β value is $\beta = 2.445$, which corresponds to 288 MeV. For each lattice, a value of T/T_c is also listed in Table I. The precise value for T_c is irrelevant for the conclusions of this section.

TABLE I. Parameters for the pure gauge simulations on a $24^3 \times 6$ lattice with the topology-fixing extra Wilson fermions (labeled as FT). The global topological charge is fixed to $Q = 0$ in these runs. Lattice spacing is estimated from the heavy-quark potential. The number of configurations used for eigenvalue calculations and the (disconnected) correlator calculations are given in the columns of $N_{\rm eigenval}$ and $N_{\rm correlators}$. Also listed are the runs without fixing topology (CT) at $\beta = 2.58$ (with the Iwasaki gauge action). The critical temperature for this case is $\sim$300 MeV [23]. The total number of configurations for this run is 1069. Out of these, the sectors of global topological charge $|Q| = 0$ and 1 are selected for measurements of the disconnected correlators.

Type	β	a (fm)	T (MeV)	T/T_c	$N_{\rm eigenval}$	$N_{\rm correlators}$
FT	2.35	0.132	249	0.86	106	106
FT	2.40	0.123	268	0.93	336	336
FT	2.43	0.117	281	0.97	101	101
FT	2.445	0.114	288	1.00	424	420
FT	2.45	0.113	290	1.01	584	584
FT	2.46	0.111	295	1.02	251	245
FT	2.48	0.107	306	1.06	420	321
FT	2.50	0.104	316	1.10	379	218
FT	2.55	0.094	348	1.20	487	487
CT	2.58 $Q = 0$	0.099	331	1.10	299	235
CT	2.58 $Q = 1$	0.099	331	1.10	262	257

B. Eigenvalue spectral density

Before analyzing the topological susceptibility, we investigate the eigenvalue distribution of the overlap Dirac operator, which is closely related to the topological susceptibility as we discuss below. Above the transition temperature the density of near-zero eigenvalues must vanish as dictated by the Banks-Casher relation [1].[1] On the other hand, a sharp peak at very low eigenvalues has been observed in previous works at or above the critical temperature [8,26,27]. These were conjectured to be related to the presence of local topological object, such as an instanton–anti-instanton pair. If this is the case, these near-zero eigenmodes should have significant contributions to the topological susceptibility.

Eigenvalues of the overlap Dirac operator (2) are calculated applying the implicitly restarted Lanczos algorithm for a chirally projected operator $P_+ D_{\rm ov} P_+$, where $P_+ = (1+\gamma_5)/2$. It gives a real part of the eigenvalue of $D_{\rm ov}$, $\mathrm{Re}\lambda_{\rm ov}$, and then the complex $\lambda_{\rm ov}$ is reconstructed by solving a relation $|1-\lambda_{\rm ov}/m_0|^2 = 1$, which is a direct consequence of the Ginsparg-Wilson relation. The complex eigenvalue $\lambda_{\rm ov}$ is projected onto the imaginary axis as $\lambda \equiv \mathrm{Im}\lambda_{\rm ov}/(1-\mathrm{Re}\lambda_{\rm ov}/2m_0)$.

When applying the overlap operator (2), we approximate the sign function using a rational approximation with the Zolotarev coefficients after subtracting a few lowest-lying eigenmodes of the kernel operator $H_W(-m_0)$. Taking the degree of the rational function to be 16th, the precision of the approximation is kept better than 10^{-10}. With this tiny error we confirmed that the low-lying eigenvalues of $D_{\rm ov}$ are obtained to eight digits or better. The precision of the approximation is kept better than 10^{-7}. Further details may be found in Ref. [13].

In Fig. 1 we plot the eigenvalue spectral density observed on pure gauge lattices. In this study, Σ is defined with the lattice regularization and not converted to the continuum regularization schemes, such as the $\overline{\rm MS}$ scheme. On the quenched lattices, the thermodynamical limit is equivalent to the infinite-volume limit, and our lattices are already sufficiently close to this limit when extracting Σ from the data. (Note that there is no long-range mode in the pure gauge theory.)

From the plot, we find that at low temperature ($\beta = 2.35$–2.43) the eigenvalues accumulate to the amount corresponding to $\pi\rho(0) \sim (200\text{–}300\ \mathrm{MeV})^3$. There is no sharp change observed at the critical temperature ($\beta = 2.445$), but $\rho(0)$ decreases towards higher temperatures and eventually vanishes at $\beta = 2.55$.

More interestingly, we confirm the presence of the peak near $\lambda = 0$ at around the critical temperature. Note that our configurations are generated in the $Q = 0$ sector and there are no exact zero modes. The near-zero modes responsible for the peak have very small eigenvalues (less than 20 MeV) but they are still nonzero. We will show that these near-zero modes give the main contribution to the topological susceptibility.

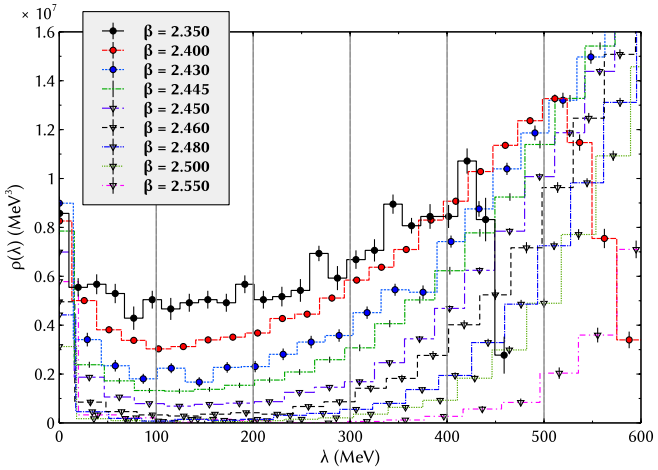

FIG. 1 (color online). Eigenvalue spectral density in quenched QCD at finite temperature. The histograms plotted with filled symbols are those below the critical temperature. Those above the critical temperature are plotted with open symbols. The data at a *would-be* critical point ($\beta = 2.445$) are shown without symbols. The error bars associated with the symbols are estimated using the jackknife method. The inset shows a magnification of the near-zero mode region, showing an accumulation of very low eigenmodes.

C. Disconnected correlation functions

So far, very few groups have studied the topological susceptibility χ_t at finite temperature in the pure SU(3) gauge theory. The most complete results are found in two papers [28,29]. Both calculated the variance of the global topological charge to obtain $\chi_t = \langle Q^2\rangle/V$. The former used the geometrical definition of the topological charge, i.e., a discretized version of $F_{\mu\nu}\tilde{F}_{\mu\nu}$, on configurations generated with the standard Wilson action. The topological susceptibility was shown to be stable around the zero-temperature value [$\sim (180\ \mathrm{MeV})^4$] until the transition temperature, where it starts decreasing. A disadvantage of the geometrical method for measuring the topological charge is that it requires some cooling steps that potentially affect the final results. The other work [29] used the Lüscher-Weisz action and directly counted the number of zero modes of a lattice Dirac operator, which approximately satisfies the Ginsparg-Wilson relation to measure the global topological charge through the index theorem. The results of these two works reasonably agree with each other. We take the numbers from Ref. [29] for a comparison with our results.

We calculate the topological susceptibility on the gauge configurations generated at a fixed global topological

[1]Strictly speaking, this is valid only when the chiral condensate is an order parameter of the phase transition. In the quenched theory, this is not absolutely necessary, but we assume it as a working hypothesis in this section.

charge using the formula (8). It requires a calculation of the disconnected quark-flow diagram, appearing in the evaluation of the correlation function $\langle mP(x)mP(0)\rangle$. Namely, we have to calculate

$$D_{55}(x,0) = \langle \mathrm{Tr}[\gamma_5 S(x,x)]\,\mathrm{Tr}[\gamma_5 S(0,0)]\rangle \qquad (10)$$

for each space-time point x. Here, $S(x,y)$ is a quark propagator obtained by an inversion of the overlap Dirac operator D_{ov} for a given source point y. Since the numerical cost for a direct calculation is too expensive, one typically uses some stochastic techniques. In this work, on the other hand, we introduce a representation of $S(x,y)$ in terms of the eigenvalues λ_k and eigenvectors $\psi_k(x)$,

$$S(x,y) = \sum_k \frac{\psi_k(x)\psi_k^\dagger(y)}{\lambda_k + m}. \qquad (11)$$

This is an exact representation when the sum is taken over all eigenmodes. We truncate the sum to include only the low-lying modes, which should dominate the long-distance correlations. We validate this approximation by inspecting the correlation functions constructed with 30, 40 and 50 low-lying eigenpairs at $\beta = 2.40$. Each eigenpair includes two terms in Eq. (11): one is from the eigenmode of λ_k and $\psi_k(x)$, and the other is that of λ_k^* and $\gamma_5\psi_k(x)$, which is also an eigenmode of D_{ov}. For the valence quark mass m in Eq. (11) we take $am = 0.01$, but the final result for the disconnected diagram is almost independent of am.

Figure 2 shows the disconnected correlator with different numbers of low-lying eigenpairs. We find that the disconnected correlation function is indeed dominated by the low-lying eigenmodes and there is no significant difference between 40 and 50. Therefore we can safely assume that the evaluation of the disconnected quark diagram using the 50 eigenpairs is sufficiently precise and adopt this procedure in the following analysis.

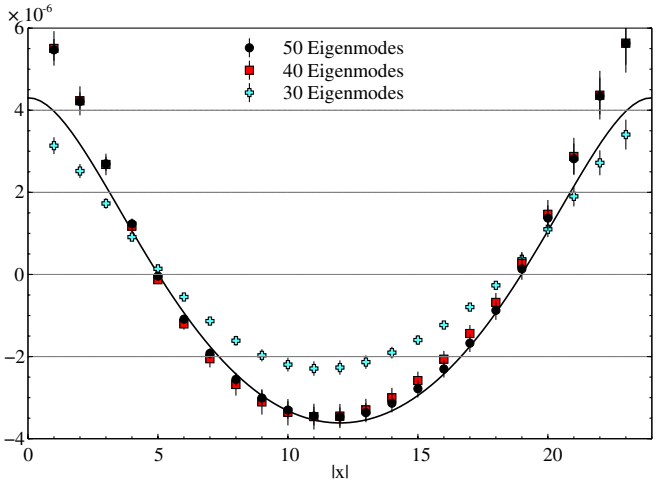

FIG. 2 (color online). Disconnected correlator approximated by different numbers of eigenmodes, i.e., 30, 40 and 50 eigenmodes. The data is at $\beta = 2.40$ and $m = 0.05$, which is below the transition temperature. The continuous line is a fit of the 50 eigenmodes' data.

On the quenched lattices, we only evaluate the disconnected quark-line contributions to the correlator, since the long-distance correlation from the pion channel does not exist in the disconnected contribution. Instead, there is a so-called "hairpin" contribution [30] of the form

$$f_P \frac{1}{p^2 + m_\pi^2} m_0^2 \frac{1}{p^2 + m_\pi^2} f_P, \qquad (12)$$

where m_π is the pion mass and f_P denotes the matrix element to annihilate a pion to the vacuum through the pseudoscalar density operator. The singlet mass parameter m_0 represents a coupling between quark loops in the quenched vacuum. In the coordinate space, it corresponds to the functional form $\sim f_P^2 m_0^2 (1 + m_\pi t)\exp(-m_\pi t)$ for zero spatial momentum. We use this function to fit the lattice data at finite temperature, taking t in the spatial direction, together with a constant term $-\chi_t/V$ representing the fixed topology effect. We neglect the subleading effect of $-c_4/(2\chi_t V^2)$ in Eq. (8). The pion mass m_π is effectively determined by combining a fit of the connected diagram with that of the disconnected diagram. The overall coefficient, such as $f_P^2 m_0^2$, is treated as a free parameter.

An example of the fit is shown in Fig. 2, which is for a lattice slightly below the critical temperature. It demonstrates that the ansatz describes the lattice data well. The underlying assumption of our analysis is that the pion channel also gives a dominant contribution at long distances at finite temperature. This is a reasonable assumption below the critical temperature T_c, and seems to be valid even above T_c as our data are well fitted.

D. Topological susceptibility

The results for the topological susceptibility χ_t obtained at a fixed global topology $Q = 0$ from the constant long-distance correlation of the flavor-singlet correlator are shown in Fig. 3. Our data are plotted by black dots, which are in good agreement with those from Ref. [29] (squared and diamonds) obtained from the Q^2 distribution.

In order to further cross-check, we also accumulated 1069 configurations without fixing the topology by eliminating the extra Wilson fermions (9). This run is carried out slightly above the transition temperature by choosing the lattice spacing $a \simeq 0.10$ fm. In Table I, it is denoted as CT. The result for χ_t obtained by counting the number of exact zero modes is plotted in Fig. 3 by a cross at around $T/T_c \simeq 1.1$, which shows a good agreement with our determination from the fixed-topology run.

It is also interesting to see the consistency of this topology-changing run by selecting configurations of a given Q and analyzing them with the method for a fixed topology. We pick up two subsets of configurations with global topological charge $|Q|$ being 0 and 1, and calculate the disconnected correlation function to extract χ_t.

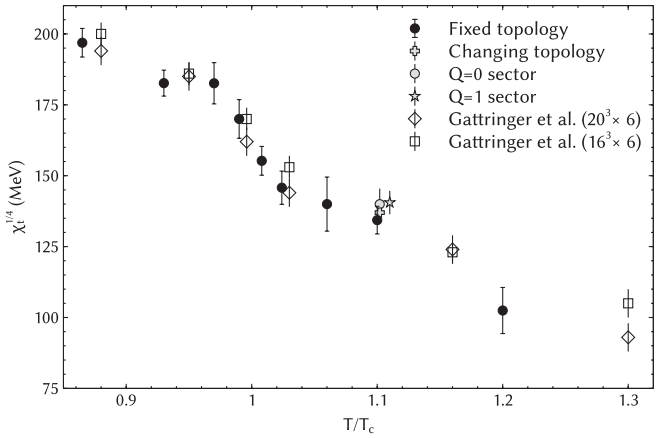

FIG. 3. Topological susceptibility in quenched QCD calculated on a $24^3 \times 6$ lattice. Data points (black dots) are obtained from a fit of the correlation functions (see text). The errors are statistical only (jacknife binned). Reference data points from Ref. [29] (but on $20^3 \times 6$ and $16^3 \times 6$ lattices) are shown by diamonds and squares. The data coming from selected sectors in a changing topology run are also shown ($Q = 1$ is slightly shifted for readability).

The results are plotted in Fig. 3 at around $T/T_c \simeq 1.1$ with different symbols. They show perfect agreement with the standard method, i.e., extracted from $\langle Q^2 \rangle / V$, as well as with the result of the fixed-topology run. This provides firm numerical evidence that the method to extract χ_t at topology-fixed configurations works as expected, at least for $\chi_t > 100$ MeV.

We also check that the eigenvalue spectral density does not depend on whether or not the configurations are generated at a fixed topological sector. The eigenvalue distribution is compared in Fig. 4. At a matched lattice spacing $a \sim 0.1$ fm, and thus at a matched temperature $T/T_c \simeq 1.1$, the spectral density at $Q = 0$ is essentially unchanged even when the configuration is generated with the constraint for the global topological charge.

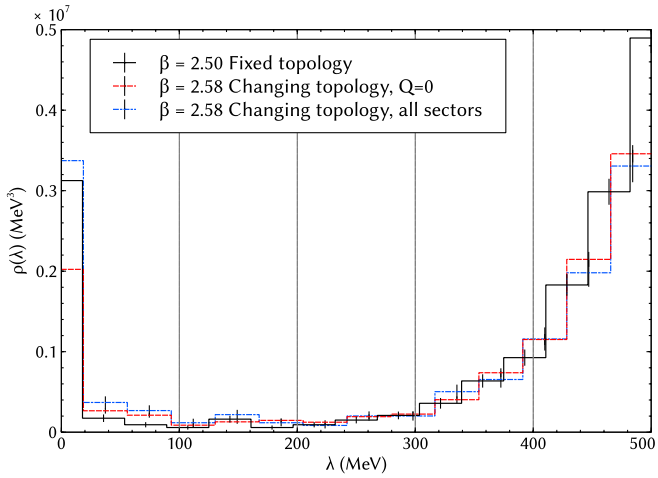

FIG. 4 (color online). Comparison of the eigenvalue spectral density from the runs with and without fixing the topology at a matched lattice spacing $a \simeq 0.1$ fm. The fixed-topology run at $\beta = 2.50$ (black, thin line) is one of those shown in Fig. 1. The result of the $Q = 0$ configurations selected out of the run without fixing the topology is overlayed (red, dashed line). These two results are in good agreement despite the slight mismatch of the lattice spacing (thus temperature). The spectral density of all configurations in the topology-changing run (thick line) show a slight deviation at the lowest bin. This is understood as an effect of the exact zero modes on the $Q \neq 0$ configurations, which are taken out in this plot. They repel the nearby eigenvalues and make the spectral density lower in the vicinity of $\lambda = 0$.

IV. DYNAMICAL QCD WITH OVERLAP FERMIONS

Given the theoretical formulation and numerical validations for the strategy to extract the $\theta = 0$ vacuum physics from the fixed-topology simulations, we embark on a dynamical simulation of finite-temperature QCD using the overlap fermion formulation. The lattice size in this exploratory study is $16^3 \times 8$ and the global topological charge is fixed to $Q = 0$.

A. Run parameters

In Table II we list simulation parameters. We use the Iwasaki gauge action together with the extra Wilson fermions and associated ghosts (9). The temporal size $N_t = 8$ is chosen to generate smooth enough gauge configurations at around the critical temperature to guarantee the locality properties of the overlap operator [31]. The aspect ratio L/N_t is not sufficiently large for a finite-temperature simulation. This is a possible source of systematic errors especially in the vicinity of the phase transition, but we do not consider such errors in this work, which is the first attempt to extract the physics related to the axial U(1) sector from the overlap fermion simulations.

Our lattice volume and statistics are not sufficient to precisely determine the transition point solely from the

TABLE II. Parameters for finite-temperature QCD simulations with two flavors of dynamical overlap fermions. The lattice size is $16^3 \times 8$. The global topology is fixed to $Q = 0$.

β	am	a (fm)	T (MeV)	T/T_c	N_{eigenval}	$N_{\text{correlators}}$
2.18	0.01	0.144	172	0.95	118	100
2.18	0.05	0.144	172	0.95	350	320
2.20	0.01	0.139	177	0.985	187	187
2.20	0.025	0.139	177	0.985	303	272
2.20	0.05	0.139	177	0.985	279	279
2.25	0.01	0.128	192	1.06	335	331
2.30	0.01	0.118	208	1.15	512	479
2.30	0.025	0.118	208	1.15	226	183
2.30	0.05	0.118	208	1.15	281	281
2.40	0.01	0.101	243	1.35	477	319
2.40	0.05	0.101	243	1.35	210	210
2.45	0.05	0.094	262	1.45	80	-

generated configurations. Instead, we assume a value of the critical temperature $T_c = 180$ MeV in two-flavor QCD. The lattice spacing is estimated from an existing analysis at zero temperature [32]. From its β value ($\beta = 2.30$), the lattice spacing in the range ($\beta = 2.18$–2.45) is obtained assuming the renormalization-group running. Systematic uncertainty associated with this estimate exists, but it does not affect the conclusion of this paper, which is qualitative.

The quark mass for degenerate up and down quarks is taken in the range 0.01–0.05 in the lattice unit. This corresponds to the bare mass of 14–70 MeV for the lattice close to the transition point ($\beta = 2.20$).

B. Dirac operator spectral density

As in our quenched analysis, we calculate the low-lying eigenvalues of the overlap Dirac operator on two-flavor QCD ensembles. Since the chiral condensate $\langle \bar{q}q \rangle$ gives an order parameter of the finite-temperature phase transition, according to the Banks-Casher relation (1) the spectral density near the zero eigenvalue provides a direct measure of the phase of the system. However, we should note that the relation holds only in the thermodynamical limit ($V \to \infty$ then $m_q \to 0$), and the results at finite volume and quark mass have to be taken with care.

For our main interest in this paper, i.e., the effective restoration of the axial U(1) symmetry, the spectral density plays a unique role. Let us consider the susceptibilities $\chi_\delta = \int d^4x \langle j^a_\delta(x) j^a_\delta(0) \rangle$ and $\chi_\pi = \int d^4x \langle j^a_\pi(x) j^a_\pi(0) \rangle$ of the isotriplet scalar and pseudoscalar operators $j^a_\delta(x) = \bar{q}(x)\tau^a q(x)$ and $j^a_\pi(x) = \bar{q}(x)\gamma_5\tau^a q(x)$. ($\tau^a$ is the Pauli matrix to specify the isospin component. We use a somewhat old notation "δ" for the isotriplet scalar state. In the modern terminology, it is called a_0.) Using the property that the eigenmodes of the Dirac operator appears as a complex-conjugate pair of λ_k and λ_k^* and with their eigenvectors simply related by γ_5, i.e., ψ_k and $\gamma_5\psi_k$, one can show that the difference of the susceptibilities is written in terms of the eigenvalues,

$$\chi_\pi - \chi_\delta = \int_0^\infty d\lambda \rho(\lambda) \frac{4m^2}{(m^2 + \lambda^2)^2}. \tag{13}$$

The disappearance of $\chi_\pi - \chi_\delta$ suggests the effective restoration of the axial U(1) above the critical temperature, or at least the anomalous violation of the axial U(1) cannot be seen in this isotriplet (pseudo)scalar channel.

In the broken phase, i.e., $\rho(0) \neq 0$, the difference (13) diverges as $1/m$ in the chiral limit, which is understood as a contribution from the long-distance correlation due to the Nambu-Goldstone pion channel. In the symmetric phase $\rho(0) = 0$, on the other hand, the difference survives under the condition $\rho(\lambda) \sim \lambda^\alpha$ with $\alpha \leq 1$. It was recently shown that this condition is not fulfilled [9], i.e., $\alpha > 2$.

For other channels, the axial U(1) restoration cannot be simply parametrized by only using the spectral function and the details of the eigenvectors are relevant. We could still expect the important role played by the near-zero modes, and it is important to identify the strength of its suppression, i.e., the power α. There is even a possibility to find a gap in $\rho(\lambda)$, i.e., zero density from $\lambda = 0$ up to some value λ_c.

For this reason, we also study the eigenvalue spectral density in two-flavor QCD. Since it requires the infinite-volume limit followed by the chiral limit, more investigation would be necessary for conclusive results. The first results obtained in this work with exact chiral symmetry would still give valuable information towards this goal.

On the configurations generated as listed in Table II, we calculate 50 lowest eigenvalues and associated eigenvectors of the Hermitian operator $\gamma_5 D_{\rm ov}$. Paired eigenmodes of $D_{\rm ov}$ can be reconstructed from them, and we effectively have 100 low-lying eigenmodes. The numerical method is the same as the one employed in the quenched study. Since the global topological charge is fixed to zero, we do not have exact zero modes.

We plot the results in Fig. 5 after rescaling them to a dimensionful unit to compare the spectra at different temperature values. We investigated the Monte Carlo histories of the lowest mode and found no evidence to suggest long autocorrelations. Also, doubling the statistics for a couple of temperatures did not significantly change the initial result.

First of all, at low temperature ($\beta = 2.18$, $T \sim 170$ MeV, top panel of Fig. 5) we find a significant number of near-zero

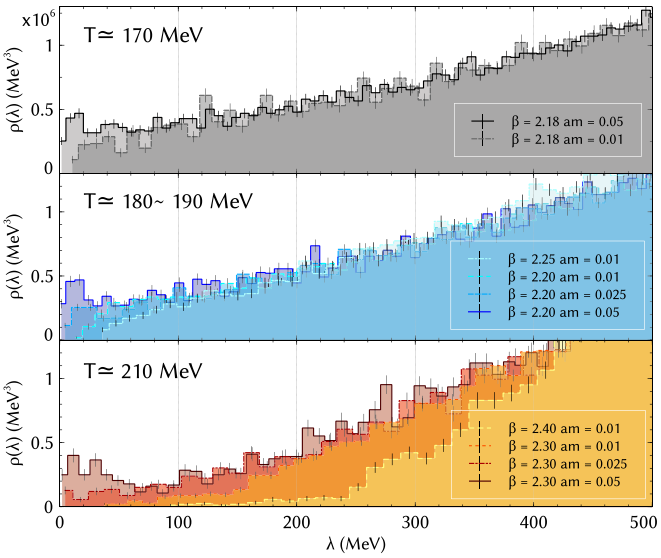

FIG. 5 (color online). Spectral density of the massless overlap Dirac operator in two-flavor QCD. Top and bottom panels are the data clearly below and above the critical temperature, respectively. The middle panel corresponds to those around the transition point. The jackknife errors are shown for each bin of the histogram. When the histogram is terminated at the lower end, it implies that we find no eigenmode below that value. The statistical error in that case is also zero, because we use the jackknife method. The lighter the color the lighter the mass.

eigenmodes suggesting $\Sigma \simeq 250$ MeV, as is known in the zero-temperature case [33,34]. Such near-zero modes found at a heavier sea-quark mass $am = 0.05$ are suppressed at $am = 0.01$. This is what should happen on a finite-volume lattice, even though we expect a nonzero density at $\lambda = 0$ in the infinite-volume limit. Such finite V and finite m_q scalings are studied in detail at zero temperature [33–36].

Near the transition temperature ($\beta = 2.20$ and 2.25, $T \sim 180$–190 MeV, middle panel of Fig. 5), the result is qualitatively unchanged. Even above the transition temperature ($\beta = 2.30$ and 2.40, $T \sim 210$ MeV, bottom panel of Fig. 5), we still see a similar number of near-zero modes when the quark mass is large ($am = 0.05$). This is consistent with our observation in the quenched theory (Fig. 1); it indicates that at the quark mass $am = 0.05$ the system is qualitatively similar to the pure gauge theory.

Once the quark mass is decreased towards the chiral limit at higher temperatures, not only the near-zero modes,

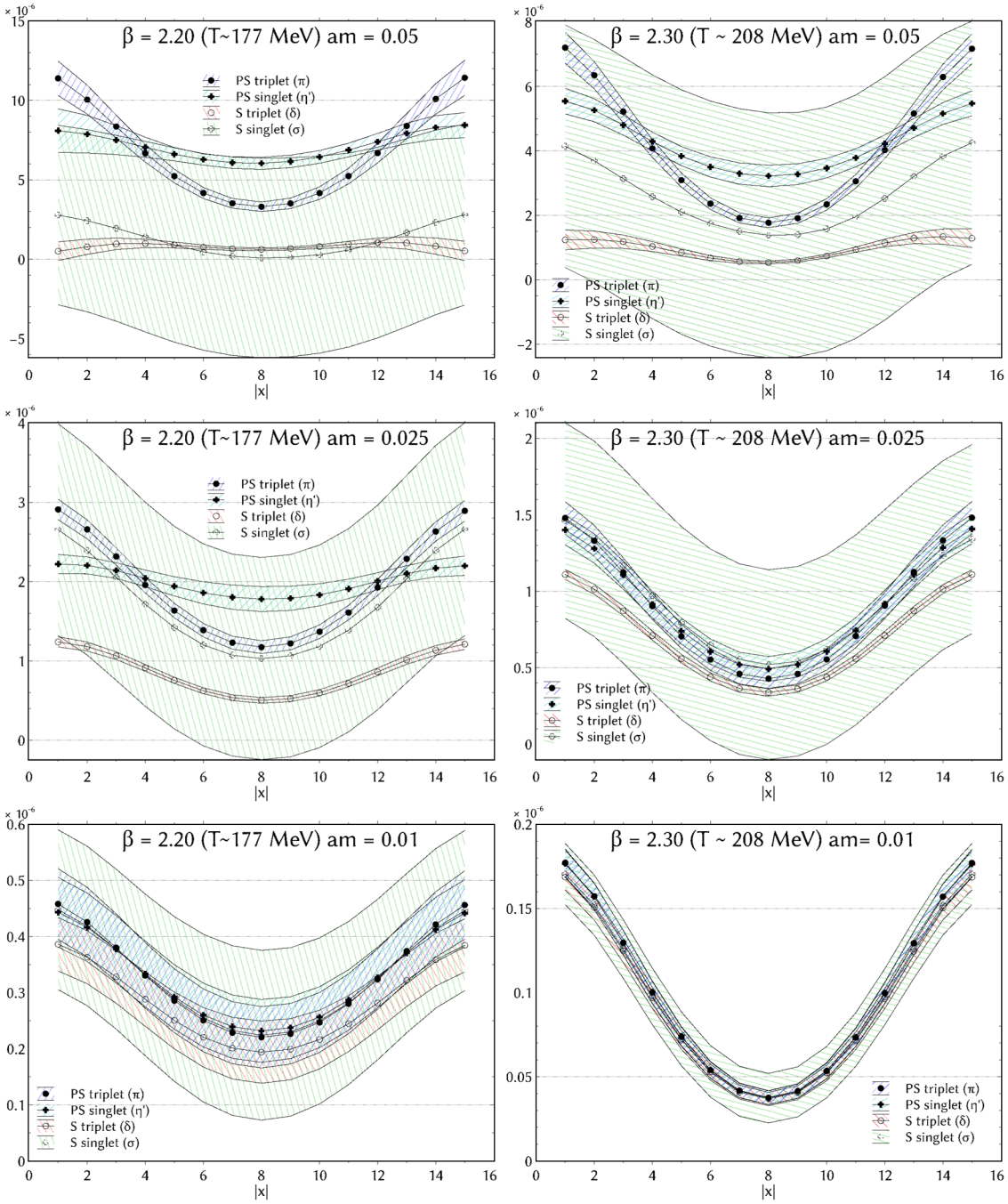

FIG. 6 (color online). Meson correlators at $\beta = 2.20$ ($T \simeq 180$ MeV) and $\beta = 2.30$ ($T \simeq 208$ MeV). Sea-quark masses are $am = 0.05$, 0.025 and 0.01. Results for the π, δ, η and σ channels are shown. Bands represent the statistical error.

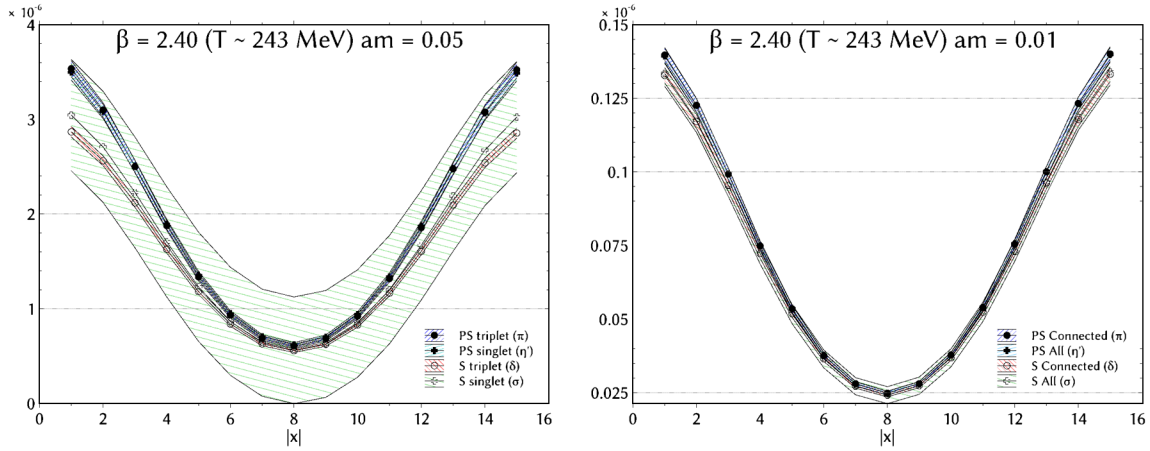

FIG. 7 (color online). Same as Fig. 6, but for $\beta = 2.40$.

say those below 10 MeV, but the modes up to ~40 MeV disappears, which is very different from what we found on the lower-temperature lattices ($T \sim 170$ MeV). Our observation suggests the following picture. In the thermodynamical limit, $\rho(0)$ disappears at the critical point (by definition). At a temperature slightly above, the suppression towards the chiral limit occurs more rapidly and at some higher temperature a gap opens. This means a stronger suppression than any power α of the form $\sim\lambda^\alpha$. Unfortunately, any quantitative argument about the power α and the point where the gap opens would not be possible with the currently available data. There is even a possibility that the gap develops right above the critical point. Much more extensive data at several quark masses and volumes would be necessary for a definite conclusion on this point.

C. Meson correlators

Further information about the restoration of the symmetry can be extracted by directly inspecting the degeneracy of meson correlators. Under the flavor-singlet (or -isosinglet) axial U(1) transformation, the pion channel is related to δ, and likewise the σ channel is related to η. On the other hand, the flavor-nonsinglet (or -isotriplet) chiral transformation connects σ to π and η to δ. Therefore, above the transition temperature we expect a degeneracy between σ and π as well as between η and δ. If the axial U(1) symmetry is effectively restored, we should see the degeneracy between σ and η as well as between π and δ. Namely, all four channels should become degenerate.

Since the difference between π and η or between σ and δ comes from the disconnected quark-flow diagram, the U(1) restoration means the absence of the disconnected diagram. The disconnected contributions to the isosinglet scalar and pseudoscalar correlators are written as

$$D(x, y) = \langle \mathrm{Tr}[S(x, x)]\,\mathrm{Tr}[S(y, y)]\rangle, \tag{14}$$

$$D_5(x, y) = \langle \mathrm{Tr}[\gamma_5 S(x, x)]\,\mathrm{Tr}[\gamma_5 S(y, y)]\rangle, \tag{15}$$

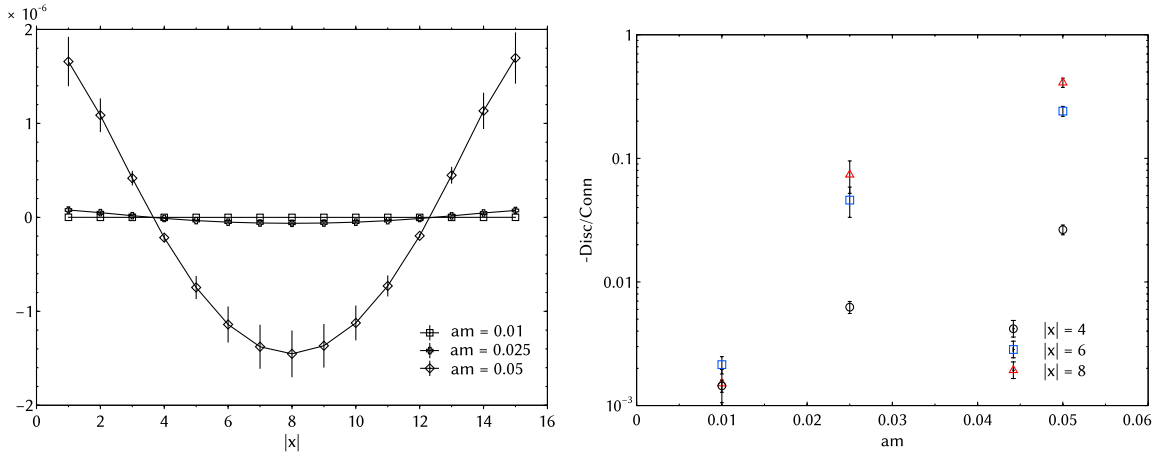

FIG. 8 (color online). (Left panel) Contribution from the disconnected diagram to the isosinglet pseudoscalar correlator. Results at three different quark masses at $\beta = 2.30$ are plotted. (Right panel) Relative contribution of the disconnected diagram to the connected is plotted in a logarithmic scale for some values of $|x|$. It shows that the disconnected contribution rapidly vanishes in the chiral limit.

where $S(x, y)$ is the quark propagator. We calculate these disconnected contributions using the eigenmode decomposition of the quark propagator (11). Only the low-lying modes that we calculated for the Dirac operator spectral density are included in this analysis. We checked that the correlators at the long distances are unchanged when the number of low modes are reduced from 50 to 40. The short-distance part is of course largely changed.

The correlation functions of the relevant mesonic channels for $am = 0.05$, 0.025 and 0.01 are plotted in Fig. 6 from top to bottom panels. The correlators are for spatial directions and averaged over other directions. The left panels show the plots at $\beta = 2.20$, slightly below the transition temperature. We find clear distinctions among different channels at $am = 0.05$ and 0.025. As the chiral limit is approached ($am = 0.01$), on the other hand, all four channels are nearly degenerate. Since the disappearance of the near-zero modes becomes significant at $am = 0.01$ (see Fig. 5, middle panel), we infer that the difference among the four mesonic channels indeed originates from the near-zero eigenmodes of the Dirac operator.

Above the transition temperature, $\beta = 2.30$ ($T \sim 210$ MeV), we find a similar degeneracy for small quark masses, as shown in the right panels of Fig. 6. At even higher temperatures, $\beta = 2.40$ ($T \sim 240$ MeV), the degeneracy is found at higher quark masses (see Fig. 7). These observations are consistent with our interpretation that the near-zero eigenmodes below, say, 20 MeV are responsible for the splitting of the chiral partners for both isosinglet and isotriplet symmetries.

Figure 8 shows the contribution of the disconnected diagram at $\beta = 2.30$. It is clear from this plot that the disconnected contribution vanishes at smaller quark masses.

V. CONCLUSIONS

The finite-temperature phase transition of two-flavor QCD could be more complicated than previously thought due to the possibility of the effective restoration of the axial U(1) symmetry. The standard analysis [3] assuming the pattern of symmetry breaking from $\mathrm{SU}(2)_L \otimes \mathrm{SU}(2)_R \otimes \mathrm{U}(1)_V$ to $\mathrm{SU}(2)_V \otimes \mathrm{U}(1)_V$ can not be directly applied if the symmetry is effectively extended to include $\mathrm{U}(1)_A$.

This work is one of the first attempts to understand the situation. Since the axial-anomaly sector of QCD is concerned, the standard technique of using the staggered fermions in lattice QCD is not appropriate for this purpose unless one approaches sufficiently close to the continuum limit. We instead used the overlap fermion formulation that exactly preserves chiral symmetry at the classical level and the $\mathrm{U}(1)_A$ is violated by the axial anomaly as in the continuum theory.

A side-effect of using the exactly chiral fermion formulation is that the global topology has to be fixed in the Monte Carlo simulation. Theoretical formulas have been developed to obtain the correct physics of the θ vacuum from such topology-fixed simulations. Essentially the error due to fixing the topology is a finite-volume effect of $O(1/V)$ and the leading $1/V$ correction can be extracted from the lattice data. We numerically tested the formula using quenched QCD at finite temperature, by calculating the topological susceptibility on the fixed-topology configurations and confirmed that the result agrees with that of the standard method.

Having established that fixing the topology at a finite temperature does not introduce unexpected systematic effects, we carried out a series of two-flavor QCD simulations on $16^3 \times 8$ lattices around the transition temperature. By measuring the eigenmodes of the overlap Dirac operator we found a gap of the spectral density in the chiral limit at high temperature, i.e., the near-zero modes disappear not just for $\lambda \simeq 0$ but also for modes of several tens of MeV. The disappearance of such near-zero modes has a correspondence with the degeneracy of the meson correlators in the channels related by the $\mathrm{U}(1)_A$ transformation, such as those between π and δ or η and σ. The origin of this degeneracy is understood: the near-zero modes are the dominant source of the disconnected-diagram contributions to the meson correlators at long distances.

This work clarifies the correspondence between the gap in the Dirac operator spectrum and the degeneracy of the meson correlators, for the first time, by the use of the overlap Dirac operator on the lattice. With other lattice fermion formulations that violate either chiral or flavor symmetry at the classical level, some ambiguity in the identification of the Dirac near-zero modes is inevitable, unless the violation of the symmetries is controlled much better than the level of 1 MeV.

For more a quantitative understanding, several sources of systematic errors are to be addressed in future works. These include the finite-volume effect and chiral extrapolation, especially near the transition point. A cross-checking of the current results with an action that allows topology change while retaining a very good chiral symmetry would also be useful. Along this line, a precise study of the order and critical exponents of the finite-temperature phase transition of two-flavor QCD, which has not been established yet, will become feasible by taking account of the effect of the axial anomaly.

ACKNOWLEDGMENTS

Numerical simulations were performed on Hitachi SR11000, SR16000 and IBM System Blue Gene Solution at KEK under the support of its Large Scale Simulation Program (No. 09/10-09, 11-05) as well as on Hitachi SR16000 at YITP in Kyoto University. This work is supported in part by the Grand-in-Aid of the Japanese Ministry of Education (No. 21674002) and by the Grant-in-Aid for Scientific Research on Innovative Areas (No. 2004: 23105710, 20105001, 20105003, 20105005) and SPIRE (Strategic Program for Innovative Research).

[1] T. Banks and A. Casher, Nucl. Phys. **B169**, 103 (1980).
[2] S. Aoki *et al.* (JLQCD and TWQCD Collaborations), Phys. Lett. B **665**, 294 (2008).
[3] R. D. Pisarski and F. Wilczek, Phys. Rev. D **29**, 338 (1984).
[4] T. D. Cohen, Phys. Rev. D **54**, R1867 (1996).
[5] N. J. Evans, S. D. Hsu, and M. Schwetz, Phys. Lett. B **375**, 262 (1996).
[6] S. H. Lee and T. Hatsuda, Phys. Rev. D **54**, R1871 (1996).
[7] M. C. Birse, T. D. Cohen, and J. A. McGovern, Phys. Lett. B **388**, 137 (1996).
[8] T. Schafer, Phys. Lett. B **389**, 445 (1996).
[9] S. Aoki, H. Fukaya, and Y. Taniguchi, Phys. Rev. D **86**, 114512 (2012).
[10] H. Ohno, U. Heller, F. Karsch, and S. Mukherjee, Proc. Sci., LATTICE (2012) 095.
[11] H. Neuberger, Phys. Lett. B **417**, 141 (1998).
[12] H. Neuberger, Phys. Lett. B **427**, 353 (1998).
[13] S. Aoki *et al.*, Prog. Theor. Exp. Phys. **2012**, 01A106 (2012).
[14] P. H. Ginsparg and K. G. Wilson, Phys. Rev. D **25**, 2649 (1982).
[15] M. Luscher, Phys. Lett. B **428**, 342 (1998).
[16] R. Brower, S. Chandrasekharan, J. W. Negele, and U. Wiese, Phys. Lett. B **560**, 64 (2003).
[17] S. Aoki, H. Fukaya, S. Hashimoto, and T. Onogi, Phys. Rev. D **76**, 054508 (2007).
[18] A. Bazavov *et al.* (HotQCD Collaboration), Phys. Rev. D **86**, 094503 (2012).
[19] G. Cossu, S. Aoki, S. Hashimoto, T. Kaneko, H. Matsufuru, J.-i. Noaki, and E. Shintani, Proc. Sci., LATTICE (2011) 188.
[20] G. Cossu *et al.* (JLQCD Collaboration), Proc. Sci., LATTICE (2012) 197.
[21] S. Weinberg, *The quantum theory of fields. Vol. 2: Modern applications* (Cambridge University Press, Cambridge, 1996).
[22] H. Fukaya, S. Hashimoto, K.-I. Ishikawa, T. Kaneko, H. Matsufuru, T. Onogi, and N. Yamada (JLQCD Collaboration), Phys. Rev. D **74**, 094505 (2006).
[23] Y. Iwasaki, K. Kanaya, T. Kaneko, and T. Yoshie, Phys. Rev. D **56**, 151 (1997).
[24] L. Del Debbio, G. M. Manca, and E. Vicari, Phys. Lett. B **594**, 315 (2004).
[25] S. Schaefer, R. Sommer, and F. Virotta (ALPHA Collaboration), Nucl. Phys. B **845**, 93 (2011).
[26] R. G. Edwards, U. M. Heller, J. E. Kiskis, and R. Narayanan, Phys. Rev. D **61**, 074504 (2000).
[27] V. Bornyakov, E. Luschevskaya, S. Morozov, M. Polikarpov, E.-M. Ilgenfritz, and M. Müller-Preussker, Phys. Rev. D **79**, 054505 (2009).
[28] B. Alles, M. D'Elia, and A. Di Giacomo, Nucl. Phys. B **494**, 281 (1997).
[29] C. Gattringer, R. Hoffmann, and S. Schaefer, Phys. Lett. B **535**, 358 (2002).
[30] W. A. Bardeen, A. Duncan, E. Eichten, and H. Thacker, Phys. Rev. D **62**, 114505 (2000).
[31] N. Yamada *et al.* (JLQCD Collaboration), Proc. Sci., LAT (2006) 060.
[32] S. Aoki *et al.* (JLQCD Collaboration), Phys. Rev. D **78**, 014508 (2008).
[33] H. Fukaya *et al.* (JLQCD Collaboration), Phys. Rev. Lett. **98**, 172001 (2007).
[34] H. Fukaya, S. Aoki, T. Chiu, S. Hashimoto, T. Kaneko, H. Matsufuru, J. Noaki, K. Ogawa, T. Onogi, and N. Yamada (JLQCD and TWQCD Collaborations), Phys. Rev. D **76**, 054503 (2007).
[35] H. Fukaya, S. Aoki, S. Hashimoto, T. Kaneko, J. Noaki, T. Onogi, and N. Yamada (JLQCD Collaboration), Phys. Rev. Lett. **104**, 122002 (2010).
[36] H. Fukaya, S. Aoki, T. W. Chiu, S. Hashimoto, T. Kaneko, J. Noaki, T. Onogi, and N. Yamada (JLQCD and TWQCD Collaborations), Phys. Rev. D **83**, 074501 (2011).